Analysis of Dynamic Engaged Characteristics of Wet Clutch in Variable Speed Transmission of a Helicopter

Authors:

Heyun Bao, Tongjing Xu, Guanghu Jin, Wei Huang

Date Submitted: 2021-05-27

Keywords: characteristics of dynamic engagement, oil film thickness, spring preload, wet clutch, variable speed helicopter transmission

Abstract:

The working principle and motion process of an aviation wet clutch are analyzed. The initial velocity before the friction pair engaged is solved. The transient Reynolds equation is modified, and an oil film bearing capacity model and a micro-convex bearing capacity model are derived. The film thickness equation between N friction pairs and a pressure-plate is derived. A dynamic engaged model of springs, pistons, friction pairs, and pressure plates are established. The torque balance equation is established of two pairs of friction pairs. The friction torque, rate of change in the oil film, and law of relative change in speed are obtained. The results demonstrate that the spring preload and the viscosity of the lubricating oil have a significant influence on the engagement characteristics. Increasing the quality of the friction plate will reduce the time of engagement, whereas the quality of the friction plate has slight effect on the friction torque characteristics and oil film thickness. The initial speed generated by the collision process will reduce the output speed, sharply increase the torque peak at the lock, and increase the shift shock.

Record Type: Published Article

Submitted To: LAPSE (Living Archive for Process Systems Engineering)

Citation (overall record, always the latest version):	LAPSE:2021.0475
Citation (this specific file, latest version):	LAPSE:2021.0475-1
Citation (this specific file, this version):	LAPSE:2021.0475-1v1

DOI of Published Version: https://doi.org/10.3390/pr8111474

processes

MDPI

Article

Analysis of Dynamic Engaged Characteristics of Wet Clutch in Variable Speed Transmission of a Helicopter

Heyun Bao *, Tongjing Xu, Guanghu Jin and Wei Huang

Laboratory of Science and Technology on Helicopter Transmission (LSTHT), Nanjing University of Aeronautics and Astronautics (NUAA), Nanjing 210016, China; xtjqwq@nuaa.edu.cn (T.X.); meeghjin@nuaa.edu.cn (G.J.); huangwei_wt@nuaa.edu.cn (W.H.)

* Correspondence: baoheyun@nuaa.edu.cn; Tel.: +86-1385-180-5472

Received: 15 October 2020; Accepted: 12 November 2020; Published: 17 November 2020

Abstract: The working principle and motion process of an aviation wet clutch are analyzed. The initial velocity before the friction pair engaged is solved. The transient Reynolds equation is modified, and an oil film bearing capacity model and a micro-convex bearing capacity model are derived. The film thickness equation between N friction pairs and a pressure-plate is derived. A dynamic engaged model of springs, pistons, friction pairs, and pressure plates are established. The torque balance equation is established of two pairs of friction pairs. The friction torque, rate of change in the oil film, and law of relative change in speed are obtained. The results demonstrate that the spring preload and the viscosity of the lubricating oil have a significant influence on the engagement characteristics. Increasing the quality of the friction plate will reduce the time of engagement, whereas the quality of the friction plate has slight effect on the friction torque characteristics and oil film thickness. The initial speed generated by the collision process will reduce the output speed, sharply increase the torque peak at the lock, and increase the shift shock.

Keywords: variable speed helicopter transmission; wet clutch; spring preload; oil film thickness; characteristics of dynamic engagement

1. Introduction

In fixed-rotor speed helicopters, it is difficult to balance the aerodynamic performance between the hovering and the high-speed forward flight. To further improve the helicopter performance, a variable speed transmission is being studied. The current variable speed technology is realized by varying the engine output speed through a control system, changing the output speed of the power turbine by adjusting the angle of attack of the engine power turbine or other geometric parameters, and adding a shifting mechanism in the transmission system. By adjusting the engine speed, the variation of the rotor speed is low and the allowable variation in speed is limited to approximately15% of the maximum running speed, which is much lower than 50% of the shifting structure; the second method requires various control systems to be installed inside the engine and a low-cost performance [1–3]. Therefore, the addition of a shifting mechanism has become the best solution to realize a change in helicopter speed. A wet clutch is a key component of the shifting system and is placed in a high-speed path to achieve a 1:1 high-speed output when hovering. The performance of the wet clutch will directly affect the output performance as the helicopter shifts [4].

Stevens [5] demonstrated the difference between aerodynamic wet clutches and wet clutches used for vehicles and designed a performance test for a variable speed drive system to provide a trend in the output shaft speed when shifting with a dry clutch. Natsumeda and Miyoshi [6] derived a Reynolds equation by considering the friction pair material, thermal effect, and surface roughness based on the average Reynolds equation proposed by Patir and Cheng. Berger [7] reduced the

Reynolds and force balance equations to the first-order differential equations of the film thickness and time. Vogel [8] established a mathematical model based on the SAE 2 test set, which includes an experimentally determined Stribeck function when considering the viscous and delay effects in the hydraulic signal, and based on the SAE 2 test set in the time and frequency domains. Hongwei [9] studied the thickness of the oil film between the friction pairs, which is the most important factor determining the transmission torque of the friction pair. The stability of the oil film thickness directly determines the stability of the load output speed. Jiahai [10] studied the fluid flow in a pair of friction pair gaps in a liquid-viscous speed-regulating clutch. Considering the centrifugal force, Coriolis force, viscosity-temperature characteristics, and the influence of the oil grooves, the transmission mechanism was studied. Lu Xi [11] established a simplified dynamic model for clutch gear shift and analyzed key parameters which affected the shift quality. The above theoretical analysis of the wet clutch does not combine the structural characteristics of the aerodynamic wet clutch, and only studies the motion of a pair of friction pairs, simplifying the motion state of the friction plate during the clutch engagement to a uniform motion without considering the process of a speed change.

In this paper, the dynamic engagement characteristics of a wet clutch arranged in a high-speed path of a helicopter transmission system are studied. According to the characteristics of an aviation wet clutch, the working principle and motion process of the aviation wet clutch are analyzed, and the spring, piston, friction pair, and pressure plate are established. The kinetic model derives the equation of the film thickness between the friction pair and the plate, as well as the force equation of the friction pair. Considering the surface roughness of the friction pair and the centrifugal force of the oil film, the transient Reynolds equation is modified and the oil film bearing capacity model and the micro-convex bearing capacity model are derived. Two pairs of friction pairs are selected for analysis. The variable-order numerical differential algorithm is used to solve the variation of oil film thickness, output speed, and friction torque of the aviation friction clutch. The friction coefficient and rate of change in the oil film thickness during the engaging process are obtained by other factors, the relative speed, and the influence of the engagement time. It is significant to improve the performance of an aviation wet clutch and improve the output performance while shifting, while providing a theoretical basis for a design optimization.

2. Working Principle of Aviation Wet Clutch

2.1. Transmission System Configuration

By consulting the relevant literature regarding variable speed transmission technologies for helicopters, the principles and design ideas for variable speed configurations are collated and analyzed. Based on the structural layout of a helicopter, the variable speed transmission system configuration of helicopter is designed, as shown in Figure 1.

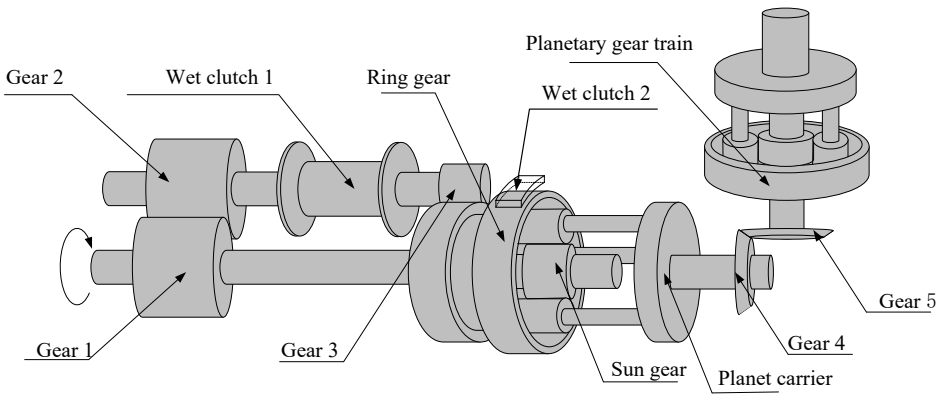

Figure 1. The variable speed transmission system configuration of helicopter

As shown in Figure 1, when in the low speed path, the power transmission path is from gear 1 to gear 2. At this time, the wet clutch 1 is engaged, the gear 3 meshes with the ring gear to transmit power, and at the same time, the gear 1 and the sun gear 1 are coaxial, and the sun gear 1 and the ring gear 1 Input power, planet carrier output, planet carrier and gear wheel 4 are coaxial, gear 4 and gear 5 mesh to transmit power, gear 5 transfers power to planetary gear system, and then planetary gear system planet carrier outputs power; When in the high-speed path, the wet clutch 1 is disconnected, the friction clutch 2 rubs against the ring gear 1, and the ring gear 1 is fixed. Only the sun gear inputs power, and the differential gear system becomes a planetary gear system, which is output through the planet carrier. The planet carrier and the gear wheel 4 are coaxial, the gear 4 meshes with the gear 5 to transmit power, the gear 5 transfers the power to the planetary gear system, and then the planetary gear system planet carrier outputs power.

2.2. Working Principle of Aviation Friction Clutch

Based on studies regarding aeronautical wet clutches, and a wet clutch designed by Stevens, in this study an aerodynamic wet clutch for a variable speed transmission system used in a helicopter is designed. A three-dimensional model is shown in Figure 2.

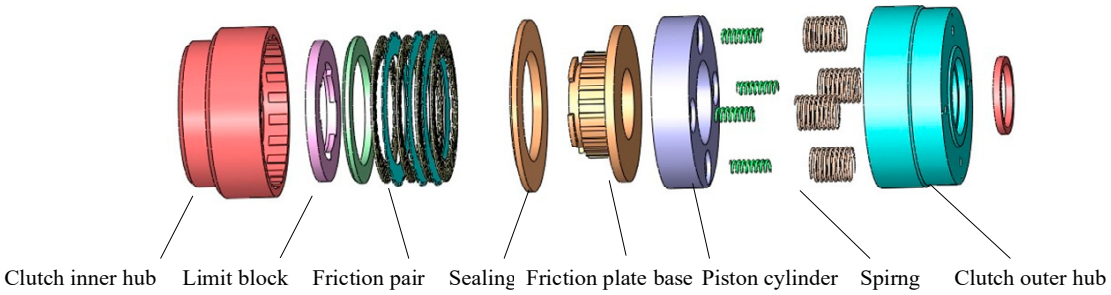

Figure 2. Three-dimensional model of a wet clutch

2.3. Analysis of Exercise Process

The movement of the friction pair includes not only the process of moving the active disk axially toward the passive disk and squeezing the oil film, but also the relative rotation of the main and passive disks and a shearing of the oil film to realize the power transmission process [12]. Combined with the structural characteristics of an aviation friction clutch, the axial movement of an aviation wet clutch is divided into three processes. During the first stage, the piston begins to relieve the pressure, the spring at an equilibrium begins to return, and the spring preload force pushes the piston against the dual steel piece. During the second stage, the piston starts to contact the dual steel piece and collides. After the piston is in contact with the steel piece, according to the structural characteristics, a plastic collision occurs. After the collision, the piston moves together with the steel piece, and the displacement and acceleration are equal. During the third stage of the piston, the dual steel piece is moved to press the friction plate. At this time, the steel piece starts to engage with the friction plate, and the engaging process is divided into three stages, the extrusion stage, the compaction stage, and the rough contact stage [13], as shown in Figure 3.

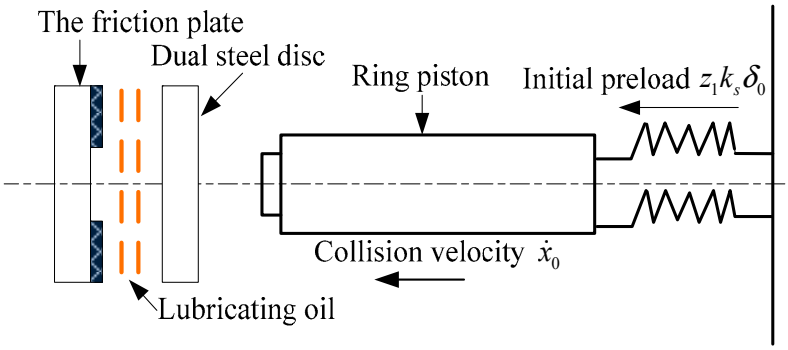

Figure 3. Pressing motion of the clutch

3. Dynamic Engagement Model

During the engaging process, the dual rigid plate and piston are engaged to the friction plate with the same acceleration under the action of the spring preload. The force analysis of the dual steel plate and the piston is carried out through an integral method: the piston and the dual steel plate are subjected to the preload of the spring, oil return pressure preventing a rapid pressure relief, oil-to-piston friction, oil film bearing capacity, and micro-convex bearing capacity are time variables related to the displacement of the dual steel sheet and the thickness of the oil film. The displacement of the dual steel sheet and the thickness of the oil film are closely related. It is necessary to further determine their relationship, and simultaneous equations are established to establish a dynamic engagement model.

3.1. Dynamic Equation of Motion

3.1.1. Oil Film Bearing Capacity Model Considering the Influence of Oil Centrifugal Force and Surface Roughness

Owing to the large speed of an aerodynamic wet clutch, the inertial force and the viscous force are of the same order, which cannot be ignored. The influence of the centrifugal force among the inertial force of the oil on the bearing capacity of the oil film must be considered. Based on the Navier-Stokes equation and the continuous equation, the Reynolds equation, which accounts for the centrifugal force of the oil, is first corrected in the cylindrical coordinate system. Next, when the friction pair is in a mixed friction stage, the oil film thickness is thinner and is on the same order of magnitude as the roughness peak height. An analysis of the oil film through a Reynolds equation will produce certain errors, and the influence of the surface roughness on the oil film needs to be considered.

The Navier-Stokes equation in the cylindrical coordinate system of a homogeneous incompressible viscous fluid with a constant viscosity is as follows:

$$\begin{cases} \frac{\partial u_r}{at} + u_r\frac{\partial u_r}{\partial r} - \frac{u_\theta^2}{r} + \frac{u_\theta}{r}\frac{\partial u_r}{\partial \theta} + u_z\frac{\partial u_r}{\partial z} = F_r - \frac{1}{\rho}\frac{\partial P}{\partial r} + \nu(\frac{\partial^2 u_r}{\partial r^2} + \frac{1}{r}\frac{\partial u_r}{\partial r} - \frac{u_r}{r^2} - \frac{2}{r^2}\frac{\partial u_\theta}{\partial \theta} + \frac{1}{r^2}\frac{\partial^2 u_r}{\partial \theta^2} + \frac{\partial^2 u_r}{\partial z^2}) \\ \frac{\partial u_\theta}{\partial t} + u_r\frac{\partial u_\theta}{\partial r} - \frac{u_r \cdot u_\theta}{r} + \frac{u_\theta}{r}\frac{\partial u_\theta}{\partial \theta} + u_z\frac{\partial u_\theta}{\partial z} = F_\theta - \frac{1}{\rho \cdot r}\frac{\partial P}{\partial \theta} + \nu(\frac{\partial^2 u_\theta}{\partial r^2} + \frac{1}{r}\frac{\partial u_\theta}{\partial r} - \frac{u_\theta}{r^2} + \frac{2}{r^2}\frac{\partial u_r}{\partial \theta} + \frac{1}{r^2}\frac{\partial^2 u_\theta}{\partial \theta^2} + \frac{\partial^2 u_\theta}{\partial z^2}) \\ \frac{\partial u_z}{\partial t} + u_r\frac{\partial u_z}{\partial r} + \frac{u_\theta}{r}\frac{\partial u_z}{\partial \theta} + u_z\frac{\partial u_z}{\partial z} = F_z - \frac{1}{\rho}\frac{\partial P}{\partial z} + \nu(\frac{\partial^2 u_z}{\partial r^2} + \frac{1}{r}\frac{\partial u_z}{\partial r} + \frac{1}{r^2}\frac{\partial^2 u_z}{\partial \theta^2} + \frac{\partial^2 u_z}{\partial z^2}) \end{cases} \quad (1)$$

where u_i is the speed of movement of the oil, $i = r,z,\theta$, η is the dynamic viscosity, ρ is the fluid density, F_i is the volume force, and P is the fluid pressure.

This study is based on the following assumptions: (1) The dynamic viscosity η is constant, independent of the temperature and pressure; (2) The fluid density ρ is constant; (3) The oil is periodically symmetrically distributed in the separation gap, that is, $\partial u_i/\partial\theta = 0$, $i = r,z,\theta$, $\partial P/\partial\theta = 0$; (4) There is no relative sliding between the oils. The velocities of the surface and oil when attached to the surface are equal, and the lubricating oil has no relative sliding in the circumferential direction at the contact interface between the friction plate and dual steel sheet, that is, $u_r(r,0) = u_r(r,H_0) = 0$,$u_\theta(r,\theta) = rw_2$, and $u_\theta(r, H_0) = rw_1$; (5) The influence of the volume force is $F_i = 0$, $i = r,z,\theta$; (6) The thickness

of the oil film is much smaller than the diameter of the friction plate, that is, h<<R, and the velocity component of the oil in the axial direction is ignored, namely, $u_z = 0$; (7) The influence of the oil groove structure on the fluid flow state is ignored; (8) The oil film thickness h is small. The oil film pressure remains unchanged in the film thickness direction, that is, $\partial P/\partial z = 0$.

Because the velocity distribution of the circumferential fluid flow of the friction pair in the direction of the gap of the friction pair is linear, it is proportional to the radius in the radial direction, and the z-direction velocity gradient is much larger than the velocity gradient in the r-direction. The speed gradient in other directions is negligible compared with the velocity gradient in the z-direction, namely,

$$\frac{\partial^2 u_\theta}{\partial z^2} = \frac{\partial^2 u_\theta}{\partial z \partial r} = 0 \tag{2}$$

According to the continuity equation in the cylindrical coordinate system,

$$\frac{\partial u_r}{\partial r} + \frac{1}{r}\frac{\partial u_\theta}{\partial \theta} + \frac{u_r}{r} = 0 \tag{3}$$

$$\frac{\partial u_r}{\partial r} + \frac{u_r}{r} = 0 \tag{4}$$

Continuing to seek partial guidance for Equation (4), the following is found:

$$\frac{\partial^2 u_r}{\partial r^2} = \frac{u_r}{r^2} - \frac{\frac{\partial u}{\partial r}}{r} = \frac{2u_r}{r^2} \tag{5}$$

According to the boundary conditions,

$$\begin{cases} u_r(r,0) = u_r(r,H_0) = 0 \\ u_\theta(r,0) = rw_2 \\ u_\theta(r,H_0) = rw_1 \end{cases} \tag{6}$$

Based on the average flow model of Patir and Cheng [14,15], considering the influence of roughness on the thickness of the lubricating oil film when the roughness of the friction surface is random, the pressure and shear flow factors are introduced. Combined with Formulas (1)–(6), the transient Reynolds equation accounting for the influence of the centrifugal force of the oil on the bearing capacity of the oil film is corrected. The transient Reynolds equation, which accounts for the influence of the centrifugal force, and surface roughness of the oil are derived as follows:

$$\frac{\partial}{r\partial r}\left[\phi_r \frac{r\overline{h}_t^3}{\eta}\left(\frac{\partial P}{\partial r}\right)\right] = \frac{\rho w_1^2}{r}\left[\frac{3}{10}\left(1 - \frac{w_2}{w_1}\right)^2 + \frac{w_2}{w_1}\right]\frac{\partial}{\partial r}\left(\frac{r^2\overline{h}_t^3}{\eta}\right) + 12\frac{\partial \overline{h}_t}{\partial t} \tag{7}$$

Equation (7) is integrated. The inlet and outlet pressure boundary conditions $\overline{P}(r = r_1) = P_0$ and $\overline{P}(r = r_2) = 0$ are substituted. The average oil film pressure is obtained in the radial direction:

$$\begin{gathered} \overline{p} = \left(\rho\frac{3w_1^2+3w_2^2+4w_1w_2}{20\phi_r} + \frac{3\mu}{\phi_r\overline{h}_t^3}\frac{d\overline{h}_t}{dt}\right)\left(r^2 - r_2^2\right) + \\ \frac{p_0 - \left(\rho\frac{3w_1^2+3w_2^2+4w_1w_2}{20\phi_r} + \frac{3\mu}{\phi_r\overline{h}_t^3}\frac{d\overline{h}_t}{dt}\right)\left(r_1^2 - r_2^2\right)}{\ln r_1 - \ln r_2}(\ln r - \ln r_2) \end{gathered} \tag{8}$$

Considering the influence of roughness on the thickness of the lubricating oil film when the frictional pair surface is randomly roughened, the local oil film thickness is as shown in Figure 4.

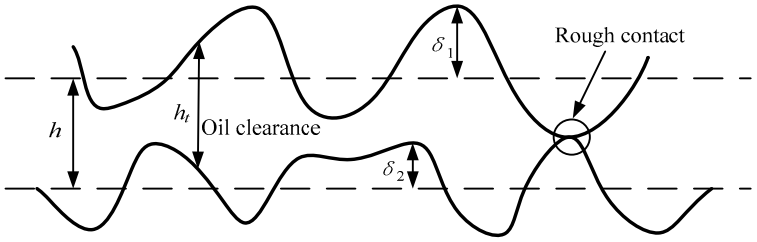

Figure 4. Local oil film thickness

The local oil film thickness expression is as follows:

$$h_t = h + \delta_1 + \delta_2 \tag{9}$$

where h is the nominal oil film thickness, m; and δ_1 and δ_2 are the roughness peak of the surface of the two friction plates, m.

The average oil film thickness is $\overline{h_t} = \int_{-h}^{\infty} (h+\delta) f(\delta) d\delta$, where $f(\delta)$ is the probability function of the standard Gaussian surface roughness peak distribution obeying the mean value of zero, and the relationship between the average oil film thickness and the nominal local oil film thickness is calculated as follows:

$$\begin{cases} \overline{h}_t = \frac{h}{2}\left[1 + erf\left(\frac{h}{\sqrt{2}\sigma}\right)\right] + \frac{\sigma}{\sqrt{2\pi}} e^{\left(-\frac{h^2}{2\sigma^2}\right)} \\ \frac{d\overline{h}_t}{dt} = \frac{d\overline{h}_t}{dh}\frac{dh}{dt} = \left\{\frac{1}{2}\left[1 + erf\left(\frac{h}{\sqrt{2}\sigma}\right)\right]\right\}\frac{dh}{dt} \end{cases} \tag{10}$$

The average radial oil film bearing capacity model that accounts for the effects of the oil centrifugal force and friction pair surface roughness is as follows:

$$\begin{cases} \overline{p} = E\left(r^2 - r_2^2\right) + \frac{P_0 - E\left(r_1^2 - r_2^2\right)}{\ln r_1 - \ln r_2}(\ln r - \ln r_2) \\ E = \rho\frac{3w_1^2 + 3w_2^2 + 4w_1 w_2}{20\phi_r} + \frac{3\eta}{\phi_r h^3} g(h)\frac{dh}{dt} \end{cases} \tag{11}$$

The integral in the area of the lubrication zone An-At, the oil film bearing capacity of the surface roughness of the friction pair, and the centrifugal force of the oil can all be taken into account. The expression is as follows:

$$\begin{cases} F_{\text{fluid}} = \iint_{A_n - A_t} P_r = (1 - \mathrm{C}) \int_0^{2\pi} d\theta \int_{r_1}^{r_2} P_r r dr = \frac{2\pi(1-\mathrm{C})\left[-E\left(r_2^2 + r_1^2\right) + 2E r_2^2 r_1^2\right]}{4} \\ + \frac{2\pi(1-\mathrm{C})\left[E\left(r_1^2 - r_2^2\right) - P_0\right]\left(r_2^2 - r_1^2\right)}{4(\ln r_1 - \ln r_2)} + 2\pi(1-\mathrm{C})E\left(r_1^4 - r_2^2 r_1^2\right) \\ + \frac{2\pi(1-\mathrm{C})P_0\left[\ln r_2\left(r_2^2 - \frac{r_1^2}{2}\right) - \frac{\ln r_1 \times r_1^2}{2}\right]}{(\ln r_1 - \ln r_2)} \\ C = A_t / A_n = n_0 \pi^2 (\eta\beta\sigma)^2 \left[-\frac{H}{\sqrt{2\pi}} e^{\frac{-H^2}{2}} - \frac{1}{2}\left(H^2 + 1\right)\left(erf\left(\frac{H}{\sqrt{2}}\right) - 1\right)\right] \end{cases} \tag{12}$$

where C is the ratio of the true contact area of the micro-protrusion to the nominal contact area; A_t is the actual contact area for rough contact, m^2; A_n is the nominal contact area, m^2; $\sigma = \sqrt{\sigma_1^2 + \sigma_2^2}$ is the root mean square of the surface roughness, m; r_1 is the inner diameter of the friction plate, m; r_2 is the outer diameter of the friction plate, m; $H = h/\sigma$ is the film thickness ratio; P_0 is the oil inlet pressure, Pa; β is the radius of curvature of the micro convex body, m; and η is the viscosity of the lubricating oil, Pa·s.

3.1.2. Film Thickness Equation between Friction Pair and Platen

The piston, friction plate, and dual steel piece are equivalent to the concentrated mass point. The variation of the oil film thickness between the N pair of friction pairs and the pressure plate is

shown in Figure 5, where m_0 is the mass of the piston, m_1–m_{n+1} are the equivalent mass of the dual steel sheet and the friction plate, 1~n + 1. In addition, H_0 is the initial gap between the friction plates, that is, the initial oil film thickness, and $x_1(t)$–$x_{n+1}(t)$ indicates the displacement of the dual steel sheet and the friction plate, 1~n+1. Here, $h_1(t)$–$h_{n+1}(t)$ are the oil film thickness between the N friction pairs.

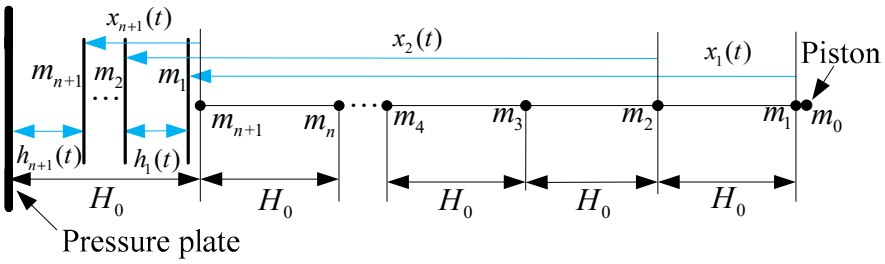

Figure 5. Variation of oil film thickness between N pairs of friction pairs and pressure plates

When the spring preload force pushes the first dual steel piece to generate a slight displacement, the thickness H_0 of the first oil film will become thinner, and the bearing capacity of the oil film will increase, thereby pushing the latter friction pair to move, reducing the thickness of the second oil film H_0. The dynamic oil film thickness equation between the N pairs of friction pairs and the pressure plate is established as follows:

$$\begin{cases} h_1(t) = H_0 - x_1(t) + x_2(t) \\ h_2(t) = H_0 - x_2(t) + x_3(t) \\ h_3(t) = H_0 - x_3(t) + x_4(t) \\ \vdots \\ h_n(t) = H_0 - x_n(t) + x_{n+1}(t) \\ h_{n+1}(t) = H_0 - x_{n+1}(t) \end{cases} \tag{13}$$

3.1.3. Friction Model of the Piston

The piston and cylinder have clearance When the piston moves axially, because the cylinder is filled with oil, the viscous resistance of the oil (the frictional force) generates a large resistance torque to the piston surface, preventing the axial movement of the piston. According to the theory of fluid mechanics, when the lubricating oil flows through the gap between two stationary parallel plates, a gap flow will be formed. The friction model of the piston will be equivalent to the gap flow of the parallel plate. The model is shown in Figure 6.

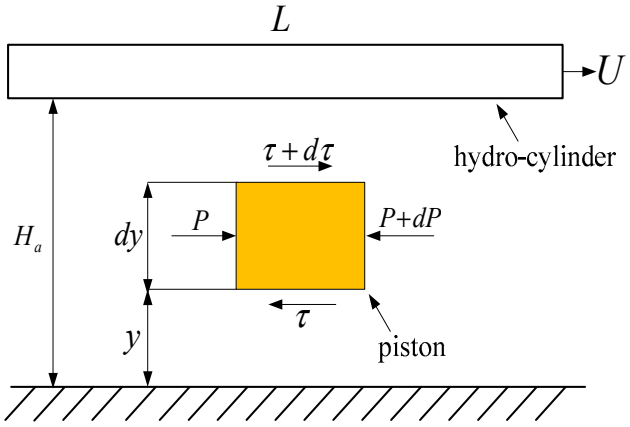

Figure 6. Friction model of the piston

The flow rate expression of the gap flow between the plates is as follows:

$$\begin{cases} u = \frac{\Delta p}{2\eta L}(H_a - y)y + \frac{U}{H_a}y \\ H_a = \psi \\ b = \pi D \end{cases} \tag{14}$$

where $\Delta p(H_a - y)y/2\eta L$ is the flow rate caused by the pressure difference between the two ends of the piston, Uy/H_a is the flow rate caused by the shearing motion generated by the fluid dragging the upper plate, ψ is the radial clearance of the piston and the cylinder sleeve, D is the diameter of the piston, Δp is the pressure difference across the piston, L is the contact length of the piston and the cylinder sleeve, b is the width of the gap, and η is the viscosity of the lubricating oil.

The internal friction stress formula of the annular gap is as follows:

$$\tau = \eta\frac{du}{dy} = \mu(\frac{\Delta P}{2\eta L}(H_a - 2y) + \frac{U}{H_a}) \tag{15}$$

Equation (15) is integrated to obtain the average friction of the oil on the piston surface:

$$\overline{F} = \frac{1}{\psi}\int_0^{\psi} \eta(\frac{\Delta P}{2\eta L}(H_a - 2y) + \frac{U}{H_a})Ady = \frac{\eta L\pi DU}{\psi} \tag{16}$$

3.1.4. Micro-Convex Contact Force Model

Under the action of the wet clutch engagement pressure, the thickness of the oil film is continuously thinned, the micro-protrusions between the friction pairs begin to contact, and the clutch engagement pressure is shared by the micro-protrusion contact bearing capacity and the oil film bearing capacity. Under actual rough contact, the roughness peak height differs according to the actual contact area of the Gauss distribution, the different contact states, and the actual rough contact area.

Greenwood and Williamson [16] proposed a dimensional normalized parameter plasticity condition to discriminate the rough peak contact state between the steel sheet and the friction lining. The formula for this is as follows:

$$\Omega = \frac{E'}{H'}\sqrt{\frac{\sigma}{\beta}} \tag{17}$$

The material of the friction pair is copper-based powder metallurgy, which considers the equivalent elastic modulus $E' = 3 \times 10^9$ pa. The root mean square of the surface roughness is $\sigma = 8.4 \times 10^{-6}$ m. The Brinell hardness value of the material is $H' = 280$ Mpa. The radius of curvature of the rough peak is $\beta = 9 \times 10^{-4}$ m. A plasticity index of $\Omega = 1.04$ is thus obtained, and the contact state of the rough peak between the dual steel sheet and the friction lining is an elastoplastic contact state. The actual contact area in the elastoplastic mixing state can be expressed as follows:

$$\begin{cases} A_t = n_0\pi^2(\eta\beta\sigma)^2A_n[-\frac{H}{\sqrt{2\pi}}e^{\frac{-H^2}{2}} - \frac{1}{2}(H^2+1)(erf(\frac{H}{\sqrt{2}}) - 1)] \\ 1 \le n_0 \le 2 \end{cases} \tag{18}$$

Patir deduced the approximate relationship between the bearing load pressure and the oil film thickness ratio of the rough contact.

$$\begin{cases} P_c(H) = 4.4086 \times 10^{-5}K'E'(4 - H)^{6.804} & H < 4 \\ P_c(H) = 0 & H \ge 4 \end{cases} \tag{19}$$

According to Equations (18) and (19), the integral of the actual working area of the friction pair micro-protrusion can be obtained, and the expression of the micro-protrusion contact force can be obtained as follows:

$$F_c = \begin{cases} \pi C({r_2}^2 - {r_1}^2)P_c & H < 4 \\ 0 & H \geq 4 \end{cases} \tag{20}$$

3.1.5. Establishment of Dynamic Equations of Motion

The motion equation of the piston and N(N = 1, 2,..., n + 1) pairs of friction pairs are established using the lumped mass method. The equivalent model is shown in Figure 7:

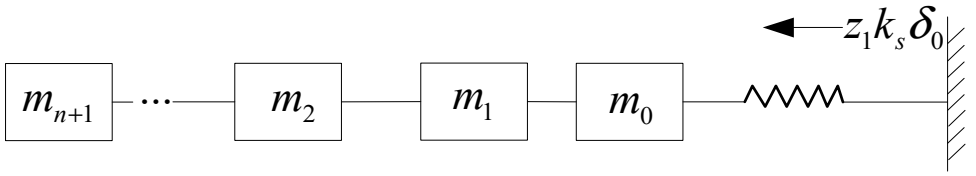

Figure 7. Equivalent model of the piston and N pairs of friction pairs

According to the structural characteristics and movement process of the aerodynamic wet clutch, the first stage is the process of the axial movement of the piston under a preload force. The equation of motion can be expressed as follows:

$$m_0\ddot{x}_0 = z_1 k_s(\delta_0 - x_0) - \overline{F}_0 - F_{load} \tag{21}$$

where m_0 is the mass of the piston, z_1 is the number of springs, δ_0 is the initial compression of the spring, x_0 is the displacement of the piston, F_{load} is the pressure of the return oil, and $\overline{F_0}$ is the frictional force of the piston.

During the second stage, the piston collides with the steel sheet and collides in an instant. According to the structural characteristics, the collision is plastic. After the collision, the piston moves with the steel sheet. The displacement and acceleration are always equal. According to the conservation of momentum, the equation is as follows:

$$m_0\dot{x}_0{}' = (m_1 + m_0)\dot{x}_0{}'' \tag{22}$$

where m_1 is the mass of the steel sheet, $\dot{x}_0{}'$ is the speed before the collision of the piston, and $\dot{x}_0''$ is the speed after the collision of the piston and the steel sheet.

During the third stage, the piston drives the dual steel piece to move together, and the friction plate is pressed under the action of the spring preloading force. At this time, the steel piece starts to engage with the friction plate, and a displacement and acceleration of the piston and first steel piece occurs during this process. Combined with the friction model of the piston, the dynamic equation of motion of N friction pairs is always equal and can be expressed as follows:

$$\begin{cases} m_0\ddot{x}_0 = z_1 k_s(\delta_0 - x_0) - \overline{F}_0 - F_{\text{load}} - F_{10} \\ m_1\ddot{x}_1 = F_{01} - F_{\text{fulid 1}} - F_{t21} \\ m_2\ddot{x}_2 = F_{\text{fulid 12}} + F_{t12} - F_{\text{fulid 32}} - F_{t32} \\ m_3\ddot{x}_3 = F_{\text{fulid 23}} + F_{t23} - F_{\text{fulid 43}} - F_{t43} \\ \overline{F}_0 = \frac{\mu L \pi D \dot{x}_0}{\psi} \\ \ddot{x}_0 = \ddot{x}_1 \\ \vdots \\ m_n\ddot{x}_n = F_{\text{fulid }(n-1)(n)} + F_{\text{t }(n-1)(n)} - F_{\text{fulid }(n+1)(n)} - F_{\text{t}(n+1)(n)} \end{cases} \tag{23}$$

where F_{fluid} is the oil film bearing capacity, and F_{t} is the micro-convex bearing capacity during rough contact.

3.2. Establishment of Friction Torque Model

The wet clutch bearing capacity is different in different engagement stages, and is mainly composed of two parts: the average oil film bearing capacity F_{fluid} and the rough contact bearing pressure F_{t}. Therefore, the friction torque of a wet clutch should also be composed of two parts: the viscous shear torque of the lubricating oil film T_{v} and the rough contact torque of the micro-convex body T_{t}. A pair of friction plate pressing discs are selected for the friction torque analysis to simulate torque transfer when multiple pairs of clutches are engaged.

3.2.1. Establishment of Torque Balance Equation

A pair of friction pairs and a pressure plate rotating at an angular velocity w_1 are taken for analysis. A torque transmission model between the dual steel piece and friction plate, and the friction plate and the pressure plate is established. The transmission torque dynamic model is shown in Figure 8.

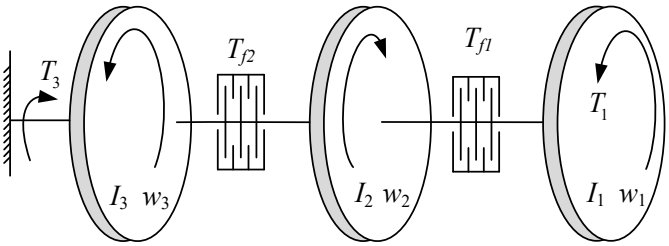

Figure 8. Transfer torque dynamics model

The torque balance equation is as follows:

$$\begin{cases} I_1 \frac{dw_1}{dt} = T_1 - T_{f1} \\ I_2 \frac{dw_2}{dt} = T_{f1} - T_{f2} \\ I_3 \frac{dw_3}{dt} = T_{f2} - T_3 \\ w_1 = w_3 \\ \frac{dw_1}{dt} = \frac{dw_3}{dt} = 0 \end{cases} \tag{24}$$

where T_1 is the input torque, T_{f1} is the transmitted torque between the steel sheet and the friction plate, T_{f2} is the transmitted torque between the friction plate and the driven plate, and T_3 is the load torque.

3.2.2. Establishment of Friction Torque Model

The total friction torque T_{f1} can be expressed as follows:

$$\begin{cases} T_{f1} = T_v + T_c \\ T_v = (1 - C)(\phi_f + \phi_{fs}) \int_0^{2\pi} \int_{r_1}^{r_2} \frac{r^2 \eta w_{rel}}{h} r dr d\theta \\ T_c = Cf \int_0^{2\pi} \int_{r_1}^{r_2} r P_c r dr d\theta \end{cases} \tag{25}$$

where $\emptyset_f$ and $\emptyset_{fs}$ are the shear factor of Patir and Cheng, f is the sliding friction coefficient. The curve formula based on the Stribeck friction coefficient model [17] is fitted to a pin disc test machine.

The rate of change of the angular velocity of the friction plate is determined as follows:

$$\frac{dw_2}{dt} = (1-C)(\phi_f + \phi_{fs})(r_2^4 - r_1^4)\frac{\pi\eta w_{rel}}{2I_2 h_1} + C(r_2^3 - r_1^3)\frac{2\pi f P_c}{3I_2} - \frac{T_3}{I_2}. \tag{26}$$

Equations (12), (13), (16), (20), and (23) are substituted into Equation (19), and combined with Equation (27), the following mutually coupled second-order ordinary differential equations of rigidity are obtained:

$$\begin{cases}
\overline{F} = \frac{1}{\psi}\int_0^{\psi} \eta(\frac{\Delta P}{2\eta L}(H_a - 2y) + \frac{\dot{x}_0}{H_a})Ady = \frac{\eta L\pi D\dot{x}_0}{\psi} \\
F_{\text{fluid21}} = \iint\limits_{A_n - A_t} P_r = (1-\mathrm{C}_1)\int_0^{2\pi} d\theta \int_{r_1}^{r_2} P_r r dr = \frac{2\pi(1-\mathrm{C}_1)[-E_1(r_2^2+r_1^2)+2E_1 r_2^2 r_1^2]}{4} \\
\quad + \frac{2\pi(1-\mathrm{C}_1)[E_1(r_1^2-r_2^2)-P_0](r_2^2-r_1^2)}{4(\ln r_1 - \ln r_2)} + 2\pi(1-\mathrm{C}_1)E_1(r_1^4 - r_2^2 r_1^2) \\
\quad + \frac{2\pi(1-\mathrm{C}_1)P_0[\ln r_2(r_2^2 - \frac{r_1^2}{2}) - \frac{\ln r_1 \times r_1^2}{2}]}{(\ln r_1 - \ln r_2)} \\
F_{\text{fluid32}} = \iint\limits_{A_n - A_t} P_r = (1-\mathrm{C}_2)\int_0^{2\pi} d\theta \int_{r_1}^{r_2} P_r r dr = \frac{2\pi(1-\mathrm{C}_2)[-E_2(r_2^2+r_1^2)+2E_2 r_2^2 r_1^2]}{4} \\
\quad + \frac{2\pi(1-\mathrm{C}_2)[E_2(r_1^2-r_2^2)-P_0](r_2^2-r_1^2)}{4(\ln r_1 - \ln r_2)} + 2\pi(1-\mathrm{C}_2)E_2(r_1^4 - r_2^2 r_1^2) \\
\quad + \frac{2\pi(1-\mathrm{C}_2)P_0[\ln r_2(r_2^2 - \frac{r_1^2}{2}) - \frac{\ln r_1 \times r_1^2}{2}]}{(\ln r_1 - \ln r_2)} \\
E_1 = \rho\frac{3{w_1}^2 + 3{w_2}^2 + 4w_1 w_2}{20\phi_r} + \frac{3\eta}{\phi_r {h_1}^3} g(h_1)\frac{dh_1}{dt} \\
E_2 = \rho\frac{3{w_1}^2 + 3{w_2}^2 + 4w_1 w_2}{20\phi_r} + \frac{3\eta}{\phi_r {h_2}^3} g(h_2)\frac{dh_2}{dt} \\
H_1 = \frac{h}{\sigma} \\
H_2 = \frac{h}{\sigma} \\
C_1 = A_t/A_n = n_0\pi^2(\eta\beta\sigma)^2[-\frac{H_1}{\sqrt{2\pi}}e^{\frac{-{H_1}^2}{2}} - \frac{1}{2}({H_1}^2+1)(erf(\frac{H_1}{\sqrt{2}}) - 1)] \\
C_2 = A_t/A_n = n_0\pi^2(\eta\beta\sigma)^2[-\frac{H_2}{\sqrt{2\pi}}e^{\frac{-{H_2}^2}{2}} - \frac{1}{2}({H_2}^2+1)(erf(\frac{H_2}{\sqrt{2}}) - 1)] \\
h_1(t) = H_0 - x_1(t) + x_2(t) \\
h_2(t) = H_0 - x_2(t) \\
F_{t21} = \begin{cases} \pi C_1({r_2}^2 - {r_1}^2)P_{c1} & H_1 < 4 \\ 0 & H_1 \geq 4 \end{cases} \\
F_{t32} = \begin{cases} \pi C_2({r_2}^2 - {r_1}^2)P_{c2} & H_2 < 4 \\ 0 & H_2 \geq 4 \end{cases} \\
\frac{dw_2}{dt} = (1-C_1)(\phi_f + \phi_{fs})(r_2^4 - r_1^4)\frac{\pi\eta w_{rel}}{2I_2 h_1} + C_1(r_2^3 - r_1^3)\frac{2\pi f P_c}{3I_2} - \frac{T_3}{I_2} \\
\ddot{x}_0 = \ddot{x}_1 \\
m_0\ddot{x}_0 = z_1 k_s(\delta_0 - x_0) - \overline{F}_0 - F_{\text{load}} - F_{10} \\
m_1\ddot{x}_1 = F_{01} - F_{\text{fulid21}} - F_{t21} \\
m_2\ddot{x}_2 = F_{\text{fulid12}} + F_{t12} - F_{\text{fulid32}} - F_{t32}
\end{cases} \tag{27}$$

In Equation (27), not only are the variables coupled to each other, the magnitudes of the physical quantities in the equation also differ significantly. The oil film change rate, output speed, and friction torque characteristics between the steel sheet and the friction plate are obtained using the variable-order numerical differential algorithm.

4. Analysis of Dynamic Engagement Characteristics

In this study, two pairs of friction pairs are selected for a dynamic engagement analysis, which makes the analysis process closer to the actual working process and the loading conditions of the aviation friction clutch. The equations are ordinary two-order differential equations with mutual coupling, and a variable-order numerical differential algorithm is used to solve the rate of change, output speed, and friction torque characteristics of the oil film between the steel sheet and the friction plate, and between the friction plate and the pressure plate. The influence of different parameters on the dynamic engagement characteristics was also analyzed. The rates of change of the oil film between the steel sheet and the friction plate, and between the friction plate and the pressure plate, were compared. The friction pair material is selected from copper-based powder metallurgy. The parameters of the simulation examples are listed in Table 1.

Table 1. Simulation parameters

Friction Pair Parameter	Symbol	Initial Value	Friction pair Parameter	Symbol	Initial Value
Friction pair inner diameter /m	r_1	0.12	Initial compression /m	δ_0	0.04
Friction pair outer diameter /m	r_2	0.16	Initial angular velocity /r/min	w_1	6000
Surface roughness root mean square /m	σ	8.4×10^{-6}	Output shaft moment of inertia /kg·m^2	I_2	2
Rough peak density /m	λ	7×10^7	Output shaft angular acceleration /rad/s^2	α_1	9
Rough peak radius of curvature /m	β	9×10^{-4}	Piston mass /kg	m_0	2
Equivalent elastic modulus /Pa	E'	3×10^9	Steel sheet quality /kg	m_1	0.367
Friction pair initial gap /m	H_0	2×10^{-4}	Friction plate quality /kg	m_2	0.367
Lubricating oil density /kg/m3	ρ	775	Piston inner diameter /m	a	0.03
Lubricating oil viscosity /Pa·s	η	0.02	Piston outer diameter /m	b	0.05
Lubricating oil inlet pressure /Pa	P_0	2×10^5	Piston length /m	L	0.2
Spring stiffness /N/m	k_s	2×10^6	Piston radial clearance /m	ψ	0.01

4.1. Analysis of Oil Film Thickness Characteristics

Figure 9 shows the curve of the oil film thickness $h_1(t)$ of the dual steel sheet and the friction plate and of the oil film thickness $h_2(t)$ of the pressure plate and the friction plate: The oil film thickness $h_1(t)$ between the pair of steel sheets and the friction plate decreases from the initial gap H_0, and the thickness of the oil film decreases sharply during the extrusion stage. A portion of the lubricating oil is squeezed out, and after the clutch enters the pressing stage, the thickness of the oil film is slowly reduced, and tends to become stable at the end of the engaging. The oil film thickness $h_2(t)$ between the friction lining and the pressure plate also decreases from the initial gap H_0, and the variation law is uniform, although the engagement time is increased by Δt_1. From this, it can be inferred that the oil film thickness between the N pairs of friction pairs will decrease synchronously from H_0, and then decrease to the same film thickness to achieve stability.

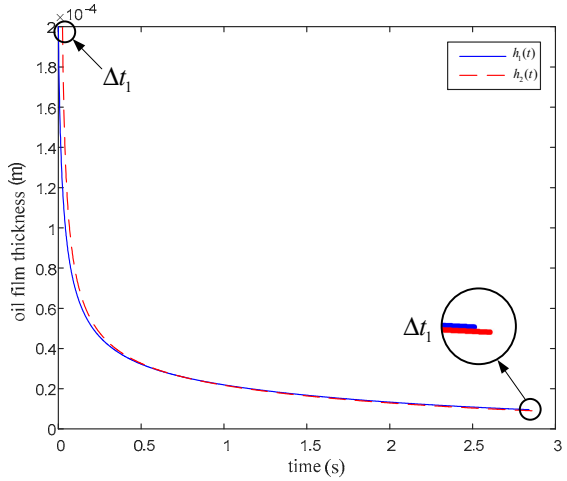

Figure 9. Curve of oil film thicknesses $h_1(t)$ and $h_2(t)$.

4.2. Analysis of Friction Torque Characteristics

Figure 10 shows the curve of viscous torque, rough contact torque, and total friction torque during the engaging process: The viscous torque increases continuously during the pressing phase, and begins to decrease during this phase until it reaches zero, where a rough torque from the compression phase begins to continuously increase. When the engagement is complete, the torque at the lock is sharply increased, forming a peak. The total friction torque is equal to the viscous torque in the pressing phase and decreases with the viscous torque. When the engagement is completed, the torque at the lock increases sharply, forming a peak and increasing the shift shock.

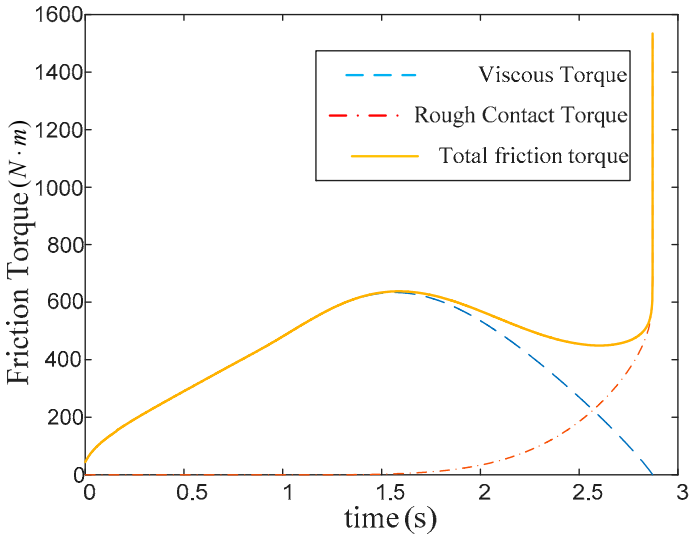

Figure 10. Friction torque curve.

4.3. Analysis of the Influence of Spring Preload

Figure 11 shows a graph of the effect of a spring preload (spring preload = spring compression) on the output speed, friction torque, and oil film thickness. It can be seen from Figure 11 that the larger the amount of spring compression, the shorter the engaging time, and the larger the output rotation speed, whereas during the pressing stage, the larger the amount of compression, the larger the viscous torque. In addition, the compression increases during the pressing and rough contact stages. The larger the rough contact torque is, the smaller the viscous torque, and the smaller the torque peak

at the lock, resulting in a small shift shock. The larger the amount of spring compression, the shorter the bonding time, and the smaller the final oil film thickness stability.

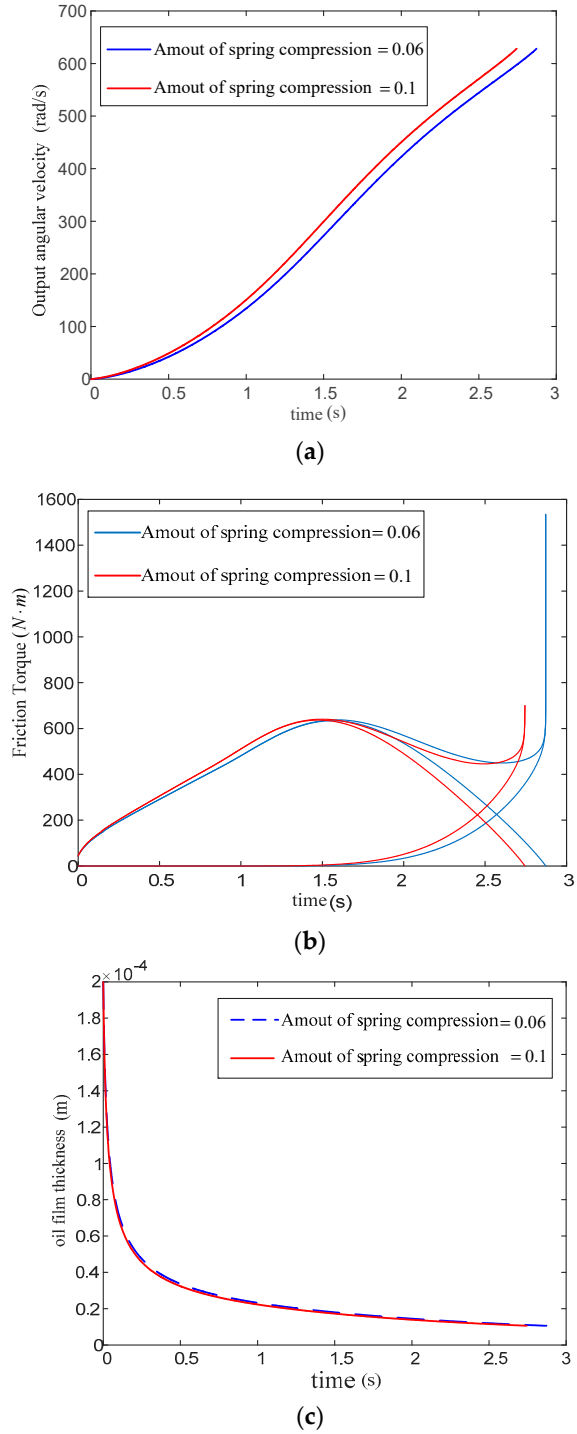

Figure 11. Effect of spring compression on output speed, friction torque, and film thickness. (**a**) Effect of spring compression on output speed; (**b**) Effect of spring compression on friction torque; (**c**) Effect of spring compression on oil film thickness.

4.4. Analysis of the Influence of Lubricant Viscosity

Figure 12 shows the effective curve of the viscosity of the lubricating oil on the output speed, friction torque, and oil film thickness: The greater the viscosity of the lubricating oil, the longer the

required engaging time, the larger the output speed, the smaller the maximum viscous torque, and the rough contact torque is smaller. The higher the viscosity, the slower the oil film thickness changes, and the final stable value of the oil film thickness is basically equal. Because the viscosity of the lubricating oil increases, the viscosity of the oil increases during the flow, and the process of entering the pressing stage slows. Therefore, the slower the change in the thickness of the oil film is, the smaller the viscosity of the lubricating oil and the faster the eventual increase in the rough torque.

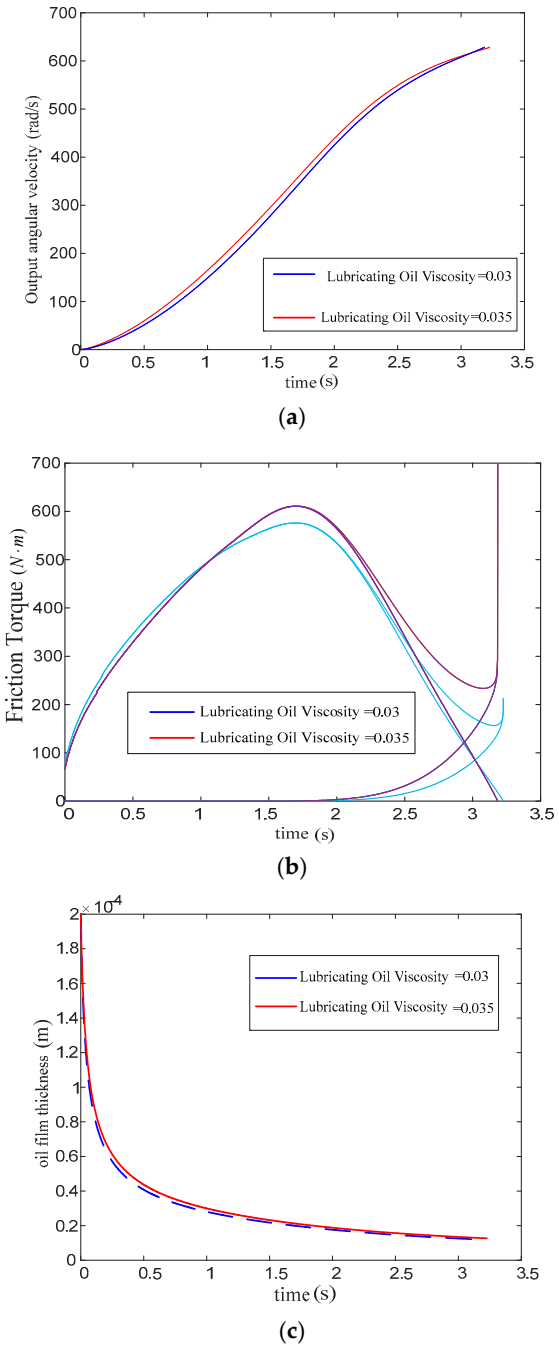

Figure 12. Effect of lubricant viscosity on the output speed, friction torque, and film thickness. (**a**) Effect of lubricant viscosity on the output speed; (**b**) Effect of lubricant viscosity on friction torque; (**c**) Effect of lubricant viscosity on oil film thickness.

4.5. Analysis of the Influence of the Initial Velocity Generated by the Collision Process

Figure 13 shows a graph of the effect of the initial velocity generated by the collision process on the output rotational speed, friction torque, and oil film thickness: When the initial velocity of the collision process is included, the engagement time is longer, the output rotational speed is larger, and there is almost no change in the thickness of the oil film. In the extrusion stage, the viscous torque is smaller. In the compression phase and the rough contact phase, the viscous torque is larger, the total friction torque is larger, but the rough contact torque is smaller; the peak torque at the lock is sharply increased, that is, the shift shock is increased.

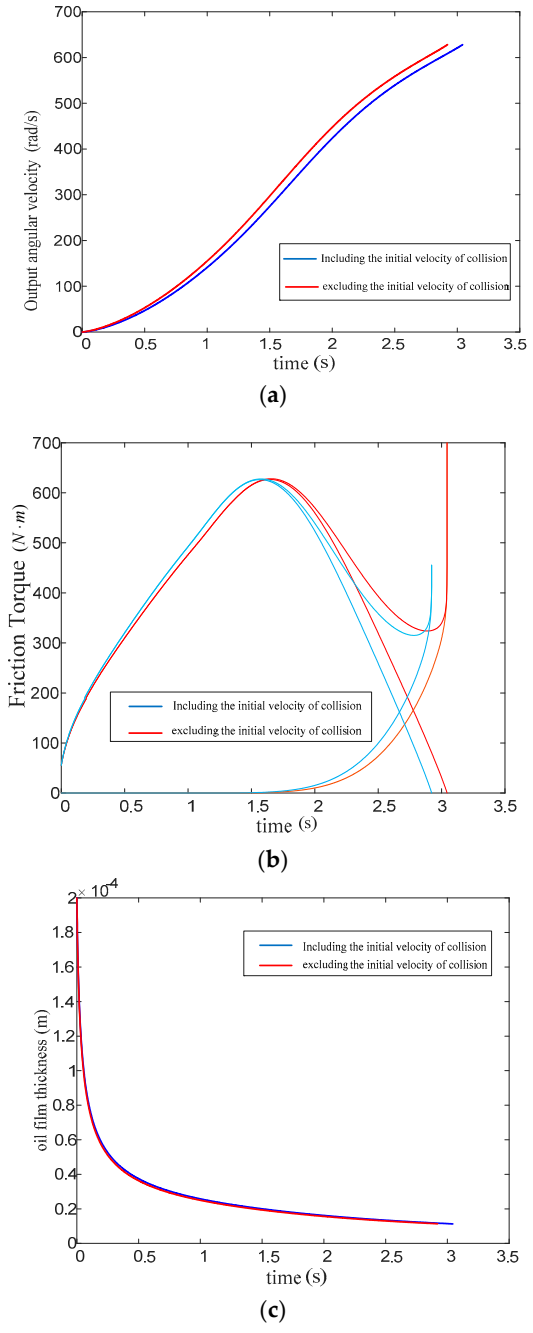

Figure 13. Effect of lubricant viscosity on the output speed, friction torque, and film thickness. (**a**) Effect of lubricant viscosity on the output speed; (**b**) Effect of lubricant viscosity on friction torque; (**c**) Effect of lubricant viscosity on oil film thickness.

4.6. Analysis of the Influence of Friction Plate Quality

Figure 14 shows the effect curve of the friction plate mass on the output speed, friction torque, and oil film thickness. The larger the friction plate quality is, the shorter the engagement time, the larger the output speed, the smaller the viscous torque, and the greater the rough contact torque. However, the difference is not great, and the quality of the friction plate has little effect on the rate of change in the thickness of the oil film.

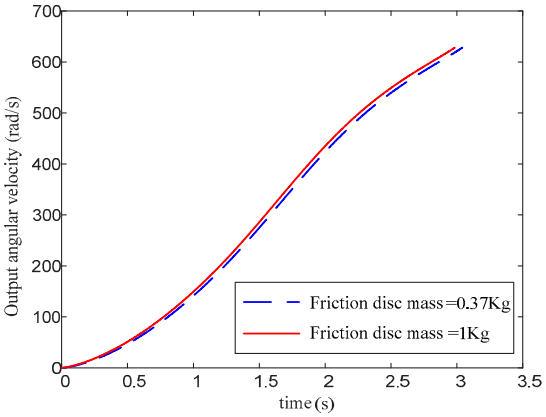

(**a**)

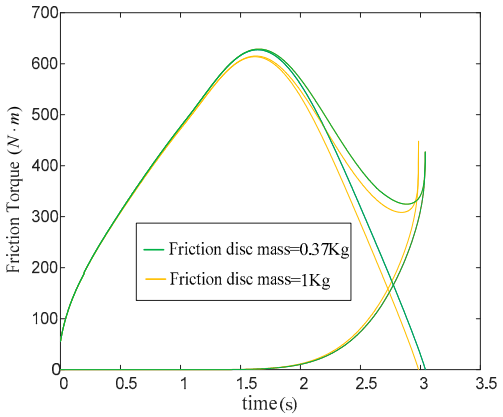

(**b**)

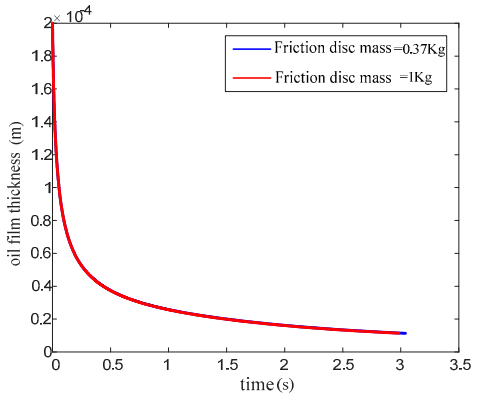

(**c**)

Figure 14. Effect of friction plate mass on output speed, friction torque, and film thickness. (**a**) Effect of friction plate mass on output speed; (**b**) Effect of friction plate mass on friction torque; (**c**) Effect of friction plate mass on oil film thickness.

5. Conclusions

A dynamic engagement model among the spring, piston, friction pair, and pressure plate was established using the concentrated mass method. A film thickness equation between the friction pair and the pressure plate and a force equation of the friction plate were derived. Two pairs of friction pairs were analyzed. The variation in oil film thickness, output speed, and friction torque of an aviation wet clutch were obtained using a variable order numerical differential algorithm. The effects of the spring preload, lubricating oil viscosity, friction plate mass, and initial velocity generated by the collision process on the friction torque, rate of change in the oil film thickness, relative rotational speed, and engagement time during the engaged process were obtained.

The results can be summarized as follows:

(1) The regularity curves of the oil film thickness $h_1(t)$ between the first pair of steel and friction plates, and the oil film thickness $h_2(t)$ between the friction and pressure plates, were obtained. These curves show the same change rule and finally a stable oil film thickness, although the required engagement time of $h_2(t)$ is shorter, from which it can be inferred that the oil film thickness between N pairs of friction pairs is sequentially reduced to the same value.

(2) The spring preload and the viscosity of the lubricating oil have a significant influence on the engagement characteristics. The larger the spring preload is, the shorter the engagement time and the higher the output speed.

(3) Increasing the quality of the friction plate will reduce the engagement time, and the quality of the friction plate has no obvious influence on the friction torque characteristics or the oil film thickness.

(4) The initial velocity of the steel plate generated during the collision process will reduce the output speed, but sharply increase the torque peak at the lock and increase the shift shock.

Author Contributions: Writing—original draft preparation, T.X.; writing—review and editing, H.B.; Data curation G.J. and W.H.; project administration, H.B.; funding acquisition, H.B. All authors have read and agreed to the published version of the manuscript.

Funding: This research was funded by the National Natural Science Foundation of China (Grant No. 51975274) and National Key Laboratory of Science and Technology on Helicopter Transmission (Nanjing University of Aeronautics and Astronautics) (Grant No. HTL-O-19G06).

Conflicts of Interest: The authors declare no conflict of interest.

References

1. Heyun, B.; Fengbo, L.; Fengxia, L. Analysis of dynamic characteristics of a variable speed helicopter transmission system. *J. Cent. South Univ.* **2019**, *50*, 2403–2416. (In Chinese)
2. Krantz, T.L.; Handschuh, R.F.; Roberts, G.D. Results of NASA Technical Challenge to Demonstrate Two-Speed Drive for Vertical Lift Vehicle. In Proceedings of the 74th AHS International Annual Forum & Technology Display, Phoenix, AZ, USA, 14–17 May 2018.
3. Hao, L.; Hui, C. Development Need and Status of Variable Speed Transmission for Helicopter. *Aeronaut. Manuf. Technol.* **2016**, *59*, 46–50. (In Chinese)
4. Stevens, M.A.; Valco, M.J.; LaBerge, K.E. Two-Speed Rotorcraft Research Transmission Power-Loss Associated with the Lubrication and Hydraulic Rotating Feed-Through Design Feature. In Proceedings of the 74th AHS International Annual Forum & Technology Display, Phoenix, AZ, USA, 14–17 May 2018.
5. Stevens, M.A.; Lewicki, D.G.; Handschun, R.F. Concepts for multi-speed rotorcraft drive system-status of design and testing at NASA GRC. In Proceedings of the American Helicopter Society (AHS) 71st Annual Forum, Virginia Beach, VA, USA, 5–7 May 2015.
6. Natsumeda, S.; Miyoshi, T. Numerical simulation of engagement of paper based wet clutch facing. *J. Tribol.* **1994**, *116*, 232–237. [CrossRef]
7. Berger, E.J.; Sadeghi, F.; Krousgrill, C.M. Analytical and numerical modeling of engagement of rough, permeable, grooved wet clutches. *J. Tribol.* **1997**, *119*, 143–148. [CrossRef]
8. Vogele, R.; Wagner, M.; Keating, M.P. Segmented and Laminated Core Steel Plate for Single and/or Double Sided Wet Clutch Friction Plates or Separator Plates. U.S. Patent 9,951,826, 24 April 2018.

9. Cui, H. *Research on the Torque Characteristic of Friction Pairs in Hydro-Viscous Clutch*; Beijing Institute of Technology: Beijing, China, 2014. (In Chinese)
10. Huang, J. *Research on the Mechanism of Fluid Power Transmission by Shear Stress in Hydroviscous Drive*; Zhejiang University: Hangzhou, China, 2011. (In Chinese)
11. Lu, X.; Wang, S.-H.; Liu, Y.-F. Application of clutch to clutch gear shift technology for a new automatic transmission. *J. Cent. South Univ.* **2012**, *19*, 2788–2796. [CrossRef]
12. Cui, J. *Research on Stability of the Soft-Start and the Mechanism of Power Transmission in Hydro-Viscous Drive*; Jiangsu University: Zhenjiang, China, 2015. (In Chinese)
13. Zhang, Z. *Study on Several Working Characteristics of Wet Clutch*; Zhejiang University: Hangzhou, China, 2010. (In Chinese)
14. Berger, E.J.; Sadeghi, F.; Krousgrill, C.M. Finite Element Modeling of Engagement of Rough and Grooved Wet Clutches. *J. Tribol.* **1996**, *118*, 137–146. [CrossRef]
15. Patir, N.; Cheng, H.S. An average flow model for determining effects of three-dimensional roughness on partial hydrodynamic lubrication. *J. Lubr. Technol.* **1978**, *100*, 12–17. [CrossRef]
16. Ciavarella, M.; Greenwood, J.A.; Paggi, M. Inclusion of "interaction" in the Greenwood and Williamson contact theory. *Wear* **2008**, *265*, 729–734. [CrossRef]
17. Liu, Y.F.; Li, J.; Zhang, Z.M.; Hu, X.H. Experimental comparison of five friction models on the same test-bed of the micro stick-slip motion system. *Mech. Sci.* **2015**, *6*, 15–28. [CrossRef]